Chemical Papers
https://doi.org/10.1007/s11696-019-00744-7

ORIGINAL PAPER

Effect of vitamin C template on morphology and structure of alumina: emerging application in enantiomer separation

Hossein A. Dabbagh[1] · Mahdieh Mozaffari Majd[1] · Fahimeh Bahrami[2] · Ali Gholami[2]

Received: 17 March 2018 / Accepted: 9 March 2019

Abstract

Mesoporous nano-aluminas were prepared using aluminium isopropoxide, vitamin C (VC as a chiral template and a co-structural directing agent with molar ratios of 50:50 and 90:10) and water. These compositions when dried at 120 °C and calcined at 250, 350 and 500 °C for 8 h under air atmosphere transformed to boehmite and γ-alumina depending on the concentration of VC. The influence of vitamin C and its degradation products on the morphology and texture of alumina was investigated by the means of XRD, FT-IR, SEM, EDX, TEM, TGA, DSC, BET and N_2 adsorption–desorption isotherm. Mesoporous aluminas possess excellent characteristics such as large surface area (ca. 394 m^2/g), 0.4 cm^3/g pore volume and narrow pore size distributions that can be synthesized through a facile and green procedure. In addition, the enantiomers of propranolol hydrochloride were successfully resolved from its racemate using $Al_{50}VC_{50}T_{350}$ ($Al_{\text{Molar ratio of the Aluminium isopropoxide}}$, $VC_{\text{Molar ratio of the Vitamin C,}}$ $T_{\text{Temperature}}$) ($R_s = 2.5$) as chiral stationary phase. The synthesis of chiral stationary phase was accomplished in a green, facile and inexpensive procedure that is of paramount importance in food and pharmaceutical industries.

Keywords Alumina · L-Ascorbic acid · Vitamin C · Template synthesis · Chiral separation · Propranolol hydrochloride

Introduction

Polymorphic aluminium oxides, generally known as alumina, have paramount importance because of their stability, high surface area and being inexpensive in a variety of industrial applications including pharmaceuticals, catalysts, ceramics, etc. (Boumaza et al. 2009; Murali and Thirumoorthy 2010; Sanchez-Valente et al. 2004), as well as adsorptive material in separation processes (Čejka 2003; Janosovits et al. 1997; Morterra and Magnacca 1996; Oberlander 1985).

In order to synthesize mesopore and macropore aluminas, several methods have been devised to achieve diverse pore size and high surface area by applying templates. Jiao and his co-workers used the mixture of cationic and anionic surfactant as template for synthesizing organized γ-alumina (Jiao et al. 2012). The pore volume of the γ-alumina prepared in this research was 0.79 cm^3/g, and its pore size was 12.1 nm, which represented excellent textural properties of this γ-alumina. Dabbagh et al. deployed alanine as a template to synthesize γ-alumina with a specific surface area of 422 m^2/g and a pore volume of 0.59 cm^3/g (Dabbagh et al. 2011). Dabbagh and Shahraki synthesized mesoporous nano-rod-shaped γ-alumina with narrow pore size distribution by utilizing phenol formaldehyde polymeric resin as a template and aluminium isopropoxide as a precursor (Dabbagh and Shahraki 2013). This method led to γ-alumina with large surface area (ca. 382 m^2/g), large pore volume and narrow pore size distributions.

Herein, aluminas were prepared using vitamin C as a chiral template. A question was raised here: Is it possible to make asymmetric chiral alumina after total or partial elimination of vitamin C? According to the work by Raman et al., elimination of the template from central structure can lead to morphological and/or stereo-chemical characteristics related to those of the template (Raman et al. 1996). Therefore, it is expected that the extraction of a chiral template

Electronic supplementary material The online version of this article (https://doi.org/10.1007/s11696-019-00744-7) contains supplementary material, which is available to authorized users.

✉ Hossein A. Dabbagh
dabbagh@cc.iut.ac.ir

[1] Catalysis Research Laboratory, Department of Chemistry, Isfahan University of Technology, Isfahan 8415483111, Iran

[2] Department of Analytical Chemistry, Faculty of Chemistry, University of Kashan, Kashan, Iran

Published online: 18 March 2019

like L-ascorbic acid produces a chiral mesoporous or nanoporous material.

To examine this, we have used the prepared aluminas as chiral stationary phase and the stock solution (1 mg/mL) of propranolol hydrochloride was passed over them using the high-performance liquid chromatography. Propranolol hydrochloride is β-adrenergic antagonists used clinically as the racemate. However, these enantiomers have different pharmacological properties and the S-(–) isomer contains the β-adrenergic blocking activity (Barrett and Cullum 1968). Since pure enantiomers achieve more effective treatment, much effort has been made to develop methods that resolve enantiomers and determine their contents efficiently. In order to resolve enantiomers, high-performance liquid chromatography (HPLC) with chiral stationary phase (CSP) is utilized. Cellulose chiral stationary phases and macrocyclic antibiotics chiral stationary phases are two kinds of CSPs used frequently for propranolol enantioseparation. These chiral stationary phases suffer from limited application in normal phase and high price (Ren-Dan et al. 2014).

To the best of our knowledge, this is the first publication which deploys vitamin C to synthesize mesoporous chiral alumina and also investigated its potential characteristic as chiral stationary phase in enantiomer resolution. Having uniform pore structures, large surface areas and narrow pore size distributions make it an ideal candidate in a wide range of catalytic processes such as adsorbents, catalysts, high-performance ceramics and catalysts supports. Due to its potential for resolving racemic mixture, it can be used as a new inexpensive home-made chiral stationary phase for propranolol enantioseparation.

Experimental

Materials

Aluminium isopropoxide (AIP), > 98.0%, was supplied by Merck, and L-(+)-ascorbic acid (99%) from Acros Organics Co. They deployed on arrival. The deionized double distilled water was prepared as the solvent in all procedures.

All reagents and solvents used for enantiomer resolution were HPLC or analytical grade. Acetonitrile and methanol of HPLC grade were supplied by Merck. Propranolol hydrochloride reference standard (RS) was purchased from USP (United States Pharmacopeia).

Synthesis of aluminas

Aluminium isopropoxide and L-ascorbic acid were dissolved in an excess amount of deionized distilled water (H_2O/Al = 10) with the molar ratios of 50:50 and 90:10, respectively, and stirred at room temperature for 1 h. The alcohol and excess water were removed at 120 °C to produce aluminium hydroxide powders.

The powders were divided into three samples. Each part was placed in the furnace at 250, 350 and 500 °C for 8 h, respectively. These samples were assigned as $Al_{\text{Molar ratio of the Aluminium isopropoxide}}$, $VC_{\text{Molar ratio of the Vitamin C}}$ and $T_{\text{Temperature}}$. For example, the sample containing 90% aluminium isopropoxide and 10% vitamin C calcined at 250 °C was named $Al_{90}VC_{10}T_{250}$.

The synthesis diagram of the composites is shown in Fig. 1.

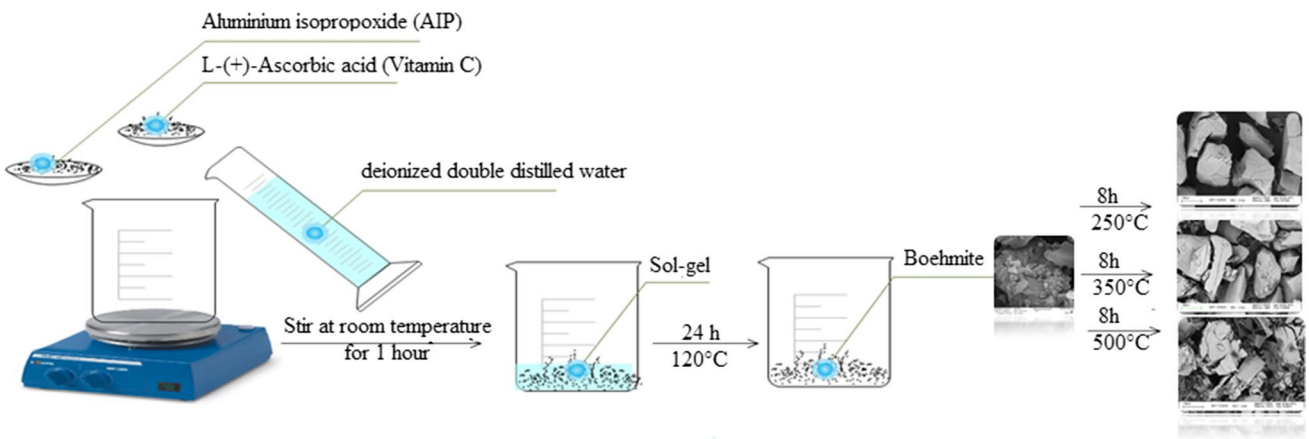

Fig. 1 Synthesis diagram of the composites

Characterization

The phase development of the samples was conducted by XRD technique (Philips Xpert instrument) with the CuKα radiation source operating at 40 kV, 30 mA, and was scanned on an angular step of 0.05° over a 2Θ range between 10 and 100°.

FT/IR-680 plus spectrometer manufactured by JASCO provided the FT-IR spectra ranged from 400 to 4000/cm.

The SEM micrographs of the nano-composite powders were carried out through a scanning electron microscope (SEM-Philips XL 30, LEO 1430VP-Carl Zeiss & Tescan Vega-3 LMU). The amplification of secondary electron signals was achieved by covering the samples with gold.

Energy-dispersive X-ray spectroscopy (EDX-Tescan Vega-3 LMU) was deployed to characterize the chemical composition of synthesized composites.

The TEM images were taken via transmission electron microscope (TEM-LEO-912AB, Carl Zeiss) to study particle size and structure of synthesized products, operating at accelerating voltage of 80 kV. Prior to TEM imaging, the samples dispersed in ethanol were placed on a carbon film supported by Cu mesh grid.

STA system, model 409 PC Luxx, was utilized to perform thermal analysis including TGA and DSC for samples under a flow of air at a rate of heating of 20 up to 1100 °C/min.

Nitrogen adsorption–desorption isotherms were obtained at − 196 °C using a BELSORP Mini II apparatus (BEL Japan company). Prior to any measurements, all the samples were passed through a flow of dry nitrogen at 150 °C for 5 h. The pore volume and specific surface area of the samples were calculated with the help of the multipoint Brunauer–Emmett–Teller (BET) procedure where the relative pressure (P/P_0) was 0.98. The pore size distributions were determined by the Barrett–Joyner–Halenda (BJH) method using the adsorption branch of the nitrogen isotherms.

Chromatographic analysis was carried out using a high-performance liquid chromatography instrument (Younglin HPLC YL9000 series) with YL9110 Pump and with autochrome 3000 software and UV–Visible detector YL9120. The filtering of mobile phase was performed by a 0.45-µm pore size filter (Merck Millipore, USA) and then passed through vacuum to be degassed.

The application of synthesized alumina in enantiomer separation

In this work, the synthesized $Al_{50}VC_{50}T_{350}$, $Al_{50}VC_{50}T_{500}$, $Al_{90}VC_{10}T_{350}$ and $Al_{90}VC_{10}T_{500}$ composites were evaluated for enantioselective separation of propranolol hydrochloride. For this purpose, these composites were used as stationary phase in a high-performance liquid chromatography to separate enantiomers. These adsorbents were grinded finely and sieved for assurance of uniform mesh size. Then, the stainless-steel HPLC columns (150 × 4.6 mm column) were packed with the fine composite. Chromatographic analysis was carried out using a high-performance liquid chromatography instrument (Younglin HPLC YL9000 series) with YL9110 Pump and with autochrome 3000 software and UV–Visible detector YL9120. The filtering of mobile phase was performed by a 0.45-µm pore size filter (Merck Millipore, USA) and then passed through vacuum to be degassed.

The elutions were carried out at ambient temperature with UV detection at 290 nm. The monograph calls for 20 µL of sample are injected with isocratic chromatographic separation using the mobile phase as prepared above at a flow rate of 1.0 mL/min. The resulting retention times indicated the potential chirality of the column.

The stock solution (1 mg/mL) was prepared by dissolving an accurately weighted amount of USP propranolol hydrochloride in minimum methanol and diluted with water. The optimized mobile phase composed of *n*-hexane/ethanol/DEA (70/30/0.3, v/v/v) was achieved at a flow rate of 1.0 mL/min and 25 °C. This solution (*n*-hexane/ethanol/DEA) was mixed and filtered (≤ 0.5 µm porosity).

The most important parameter, which is considered in this section, is resolution (R_s). Resolution in chromatography refers to the ability of column in separating two peaks. It is defined as follows:

$$R_s = \frac{2\left(t_{R_2} - t_{R_1}\right)}{\left(W_1 + W_2\right)},$$

where t_{R_1} and t_{R_2} are the retention time of peak 1 and peak 2. W_1 and W_2 are width of peak 1 and peak 2.

In this case, these two peaks are the peaks of *R*- and *S*-enantiomers of 2-propranolol. Usually, when R_s is greater than 1, it indicated the good separation of peaks.

Typical diagram for enantiomer separation using HPLC is shown in Fig. 2.

Results and discussion

L-ascorbic acid possesses six Lewis base sites, including a lactonic oxygen, C=O group and four hydroxyl groups. There is a possibility for each of six basic sites to interact with acidic sites through a covalent bond (coordinate covalent bond) as well as strong hydrogen bonding (quasi-covalent bond) in alumina (both clusters of aluminium hydroxide and aluminium oxyhydroxide), resulting in an acid–base complex. More research is needed to rationalize the role of the template in the formation of pore system in each specific case. Here, L-ascorbic acid interacts with alumina via each of

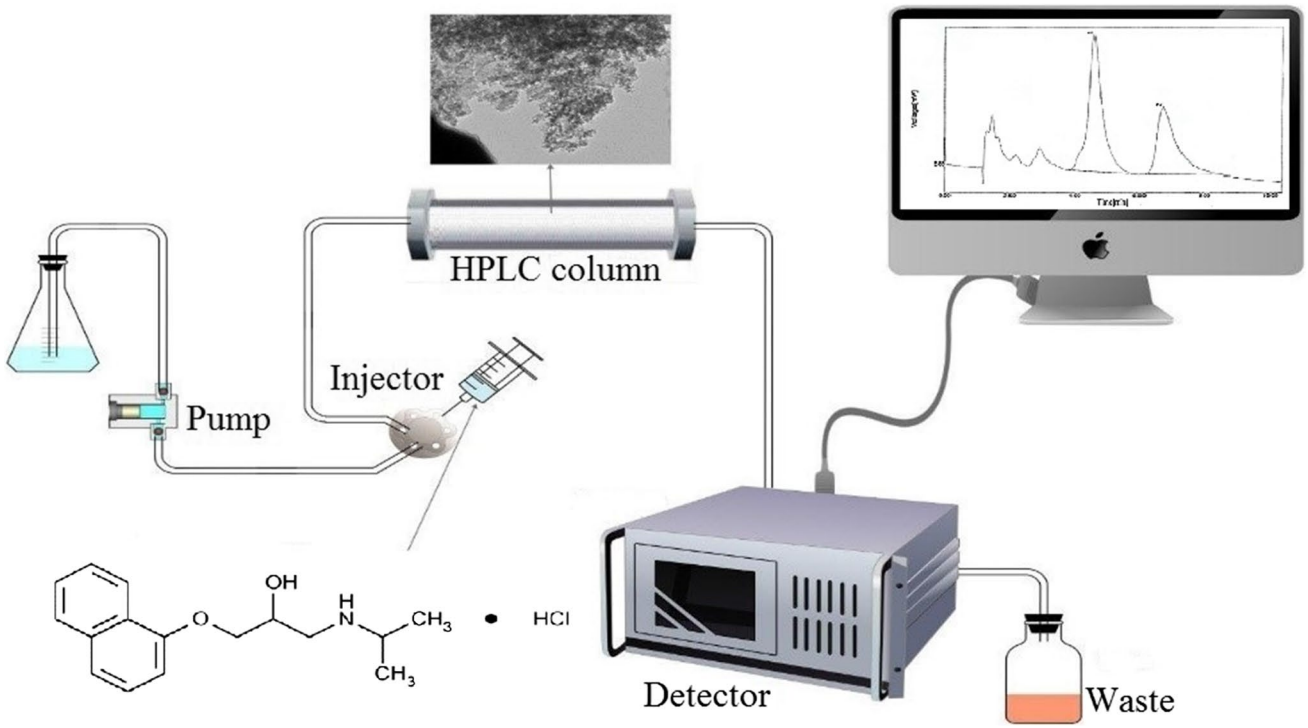

Fig. 2 Typical diagram for enantiomer separation using HPLC

six basic sites and/or acidic hydrogens, having the minimum distance to the alumina surface, and interacts and/or forms bond with alumina species where mesopores and their size are originated.

X-Ray powder diffraction

The XRD pattern was used to study the structure of composites and the grain size of crystals as shown in Fig. 3. The XRD patterns of $Al_{50}VC_{50}$ (Fig. 3a) reflect completely amorphous properties at all temperatures. Probably, the excess VC prevents the formation of a crystalline pattern. The broad diffraction peaks of these samples lead to small particle sizes and poor crystallinity. This effect was reduced for $Al_{90}VC_{10}$. The nano-size nature of these composites reveals broad diffraction peaks (Potdar et al. 2007). The characteristics of XRD patterns of $Al_{90}VC_{10}$ (Fig. 3b) confirm γ-Al_2O_3 at calcination temperatures of 350 and 500 °C (according to JCPDS card number 01-075-0921), AlO(OH) (boehmite) at 120 °C and $Al_2O_3.H_2O$ at 250 °C. The composite heated at 120 °C somewhat resembles boehmite structure (reduced crystallinity) with an orthorhombic unit cell (JCPDS card number 01-083-2384). This sample calcined at 250 °C shows transition of AlO(OH) to $Al_2O_3.H_2O$ (JCPDS card number 00-001-0774). The average size of crystallite was calculated as 5.20, 3.95, 2.38 and 4.33 nm for $Al_{90}VC_{10}T_{120}$, $Al_{90}VC_{10}T_{250}$, $Al_{90}VC_{10}T_{350}$ and $Al_{90}VC_{10}T_{500}$ by Scherrer equation, respectively (Ibrahim and Abu-Ayana 2009) (Table 1). The phase analyses patterns of samples calcined at different temperatures of 250, 350 and 500 °C are shown in supplementary Fig. S1 (Electronic Supplementary Information).

FT-IR spectra

The FT-IR spectra of Al/vitamin C composites were used to further characterize alumina–VC transitions at different calcination temperature (Figs. 4, 5). The FT-IR spectrum of $Al_{50}VC_{50}$ calcined at 120 °C (Fig. 4) shows a footprint of vitamin C at 1700/cm, corresponding to the stretching vibrations of C=O (Panicker et al. 2006). This indicates that heating the mixture to values higher than 120 °C incorporate and/or degrade the vitamin C in the synthesized composites. The broadband at 3350–3650/cm is attributed to the stretching vibration of the OH-group-adsorbed molecular H_2O (Bowen et al. 1990; Zhang and Binner 2002). The spectra of sample calcined at 120 and 250 °C show increased intensity of the new bands at 1500–1700/cm. These bands are attributed to coordinative bond between physically adsorbed water molecules and incompletely coordinated aluminium ions on the oxide surface (Vlaev et al. 1989). These bands were reduced at 350 and 500 °C. Characteristic bands of boehmite are represented in the spectra of sample calcined at these temperatures. As the peak at 1068/cm is

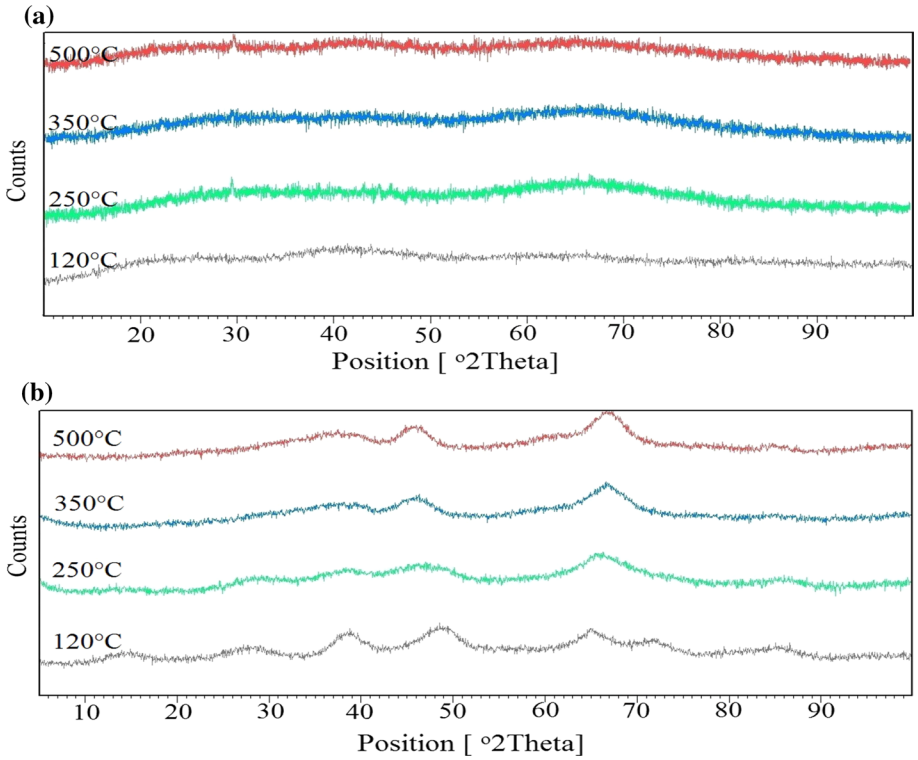

Fig. 3 XRD patterns of aluminas samples, **a** $Al_{50}VC_{50}$ and **b** $Al_{90}VC_{10}$

Table 1 Crystal sizes of the composites calculated by Scherrer equation

Sample	Scherrer equation/nm
$Al_{90}VC_{10}T_{120}$	5.20
$Al_{90}VC_{10}T_{250}$	3.95
$Al_{90}VC_{10}T_{350}$	2.38
$Al_{90}VC_{10}T_{500}$	4.33

regarded as the Al–OH–Al bending vibration, it corresponds to the crystallinity of the boehmite (Barzegar-Bafrooei and Ebadzadeh 2011) However, this peak is not very obvious at 250 °C. The bands from 400 to 750/cm are related to the bending and stretching vibration modes of AlO_6. The spectra of calcined powders at temperatures 350 and 500 °C confirm the presence of γ-alumina (Dabbagh et al. 2010; Petrovic et al. 2003) in accordance with developing peaks between 500 and 1000/cm. The peak in the range 500–650/cm was ascribed to υ-AlO_6, and the peak in the range of 700–900/cm was attributed to υ-AlO_4(Urretavizcaya et al. 1998). These

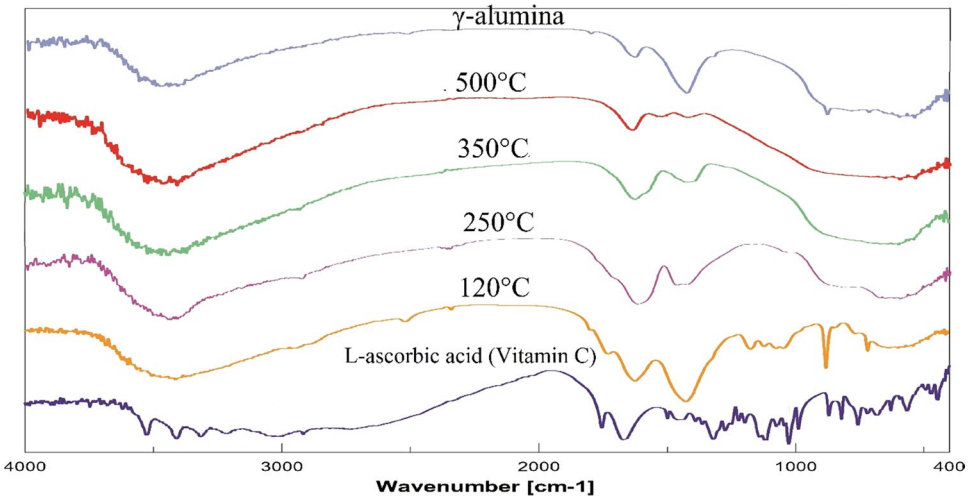

Fig. 4 FT-IR spectra of $Al_{50}VC_{50}$ composites and VC

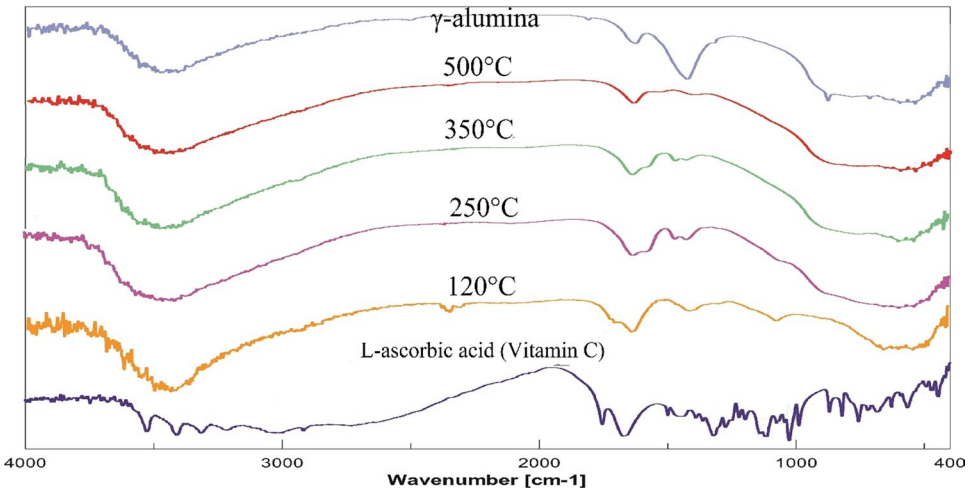

Fig. 5 FT-IR spectra of $Al_{90}VC_{10}$ composites and VC

results indicate the presence of tetrahedral and octahedral structures in γ-alumina phase. However, these results do not comply with those XRD.

FT-IR spectrum of $Al_{90}VC_{10}$ (Fig. 5) at 120 °C similar to $Al_{50}VC_{50}$ shows smaller footprint of vitamin C at 1700/cm, corresponding to the stretching vibrations of C=O. This trace shows a steady decrease at higher temperatures. The stretching vibration of the OH group connected to Al–OH group and that of adsorbed molecular H_2O and/or VC hydroxyl groups appear as the broadband at 3350–3650/cm. The peak at 1067/cm is characteristic band revealing the crystallinity of the boehmite and is represented in the spectra of sample calcined at 120 °C attributed to the Al–OH–Al bending vibration. This peak is not observed at 250 °C, since in accordance with XRD result, it is in Al_2O_3•H_2O form not AlO(OH). The advent of alumina at temperatures 350 and 500 °C occurs as this peak disappears in the calcined samples. These findings match with those of XRD. As mentioned for $Al_{50}VC_{50}$, the bands from 400 to 750/cm are related to the bending and stretching vibration modes of AlO_6. Formation of γ-alumina is carried out by dehydroxylation due to calcination of boehmite. The spectra of calcined powders at temperatures 350 and 500 °C confirm the presence of γ-alumina in accordance with the developing peaks between 500 and 1000/cm. The peak in the range 500–650/cm was ascribed to υ-AlO_6, and the peak in the range of 700–900/cm was attributed to υ-AlO_4. These results indicate the presence of tetrahedral and octahedral structures in γ-alumina phase.

The findings of TGA and DSC analysis strongly comply with those of the above-mentioned results, leading to significant water loss at 250–600 °C, which will be explained in detail in the corresponding section. In addition, absorption patterns are in agreement with the results of previous research (Dabbagh and Zamani 2011; Gandhi et al. 2010; Kim et al. 2010; Priya et al. 1997).

SEM and TEM studies

SEM and TEM analyses were recorded to characterize morphologic changes and the sizes of the synthesized samples. The SEM images of mesoporous aluminas for $Al_{50}VC_{50}T_{350}$ are depicted in Fig. 6. The SEM images of mesoporous aluminas for $Al_{50}VC_{50}T_{350}$ and $Al_{90}VC_{10}$ under thermal treatment at different temperatures of 120, 250, 350 and 500 °C are shown in Figs. S2 and S3 in (Electronic Supplementary Information). Due to topotactic nature of the solid transition of boehmite to alumina, the morphology of boehmite is kept identical to the morphology of γ-alumina (Volpe and Boudart 1985). Since the aluminium isopropoxide was dissolved in a polar solvent like water, the spherical particles could not be attained (Liu et al. 2009). Elongated and flat-shaped particles with a porous surface are witnessed in the mesoporous alumina powders, in which interparticle voids are discernible in SEM micrographs. The platy crystallites with small elongated pores coalesced in a particular shape.

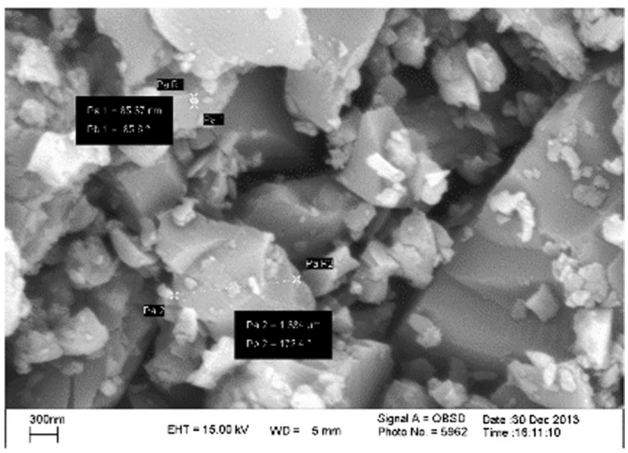

Fig. 6 SEM images of $Al_{50}VC_{50}$ T_{350}

As the vitamin C molar ratio increased, the corrugations on the external surface of agglomerates got rather rough, leading to a smaller surface area. Also, the surface structure is maintained with the less porous surface.

The chemical compositions of Al/VC products were identified by EDX analysis (Table 2). These analyses indicate that the remains of vitamin C destruction products disappeared as the temperature increased. The EDX patterns of mesoporous aluminas at different temperatures are shown in Figs. S4 and S5 (Electronic Supplementary Information).

The TEM micrographs (Fig. 7) show the morphology of mesoporous alumina for $Al_{50}VC_{50}$ at 350 °C and 500 °C and for $Al_{90}VC_{10}$ under a calcination temperature of 500 °C. Both rod-like and closely packed platelet-like particles in $Al_{50}VC_{50}$ sample at 350 °C (Fig. 7a) could be observed. The dimension of rod-like crystallites is about 100 nm length and 20 nm widths. The closely packed platelet-like particles are with the mean diameter of 20 nm. In $Al_{50}VC_{50}$ sample at 500 °C (Fig. 7b), the rod-like crystallites with a length of roughly 300 nm and width of 100 nm are clearly discernible and the aggregates of overlapping plates are at higher magnification. For Al_{90} VC_{10} sample (Fig. 7c), the crystallites resemble the morphology of agglomerates of closely packed platelet-like particles and ink-bottle pores.

Thermal gravimetric analysis

The thermal gravimetric behaviour of the boehmite was utilized to gather information about the pattern of VC loss. The TGA–DSC curves of as-prepared Al/VC composite for $Al_{50}VC_{50}$ and $Al_{90}VC_{10}$ are presented in Fig. 8. The thermogram for $Al_{50}VC_{50}$ (Fig. 8a) demonstrates the weight

Table 2 Relative percentage of chemical composition of the synthesized composites calculated by EDX (all data are reported in terms of mass fraction)

T/ °C	$Al_{50}VC_{50}$			$Al_{90}VC_{10}$		
	Carbon	Oxygen	Aluminium	Carbon	Oxygen	Aluminium
120	29.22	58.70	12.08	5.87	72.84	21.29
250	12.22	71.51	16.27	3.34	70.13	26.53
350	3.26	72.89	23.85	1.90	71.32	26.78
500	2.81	75.06	22.13	1.60	67.82	30.58

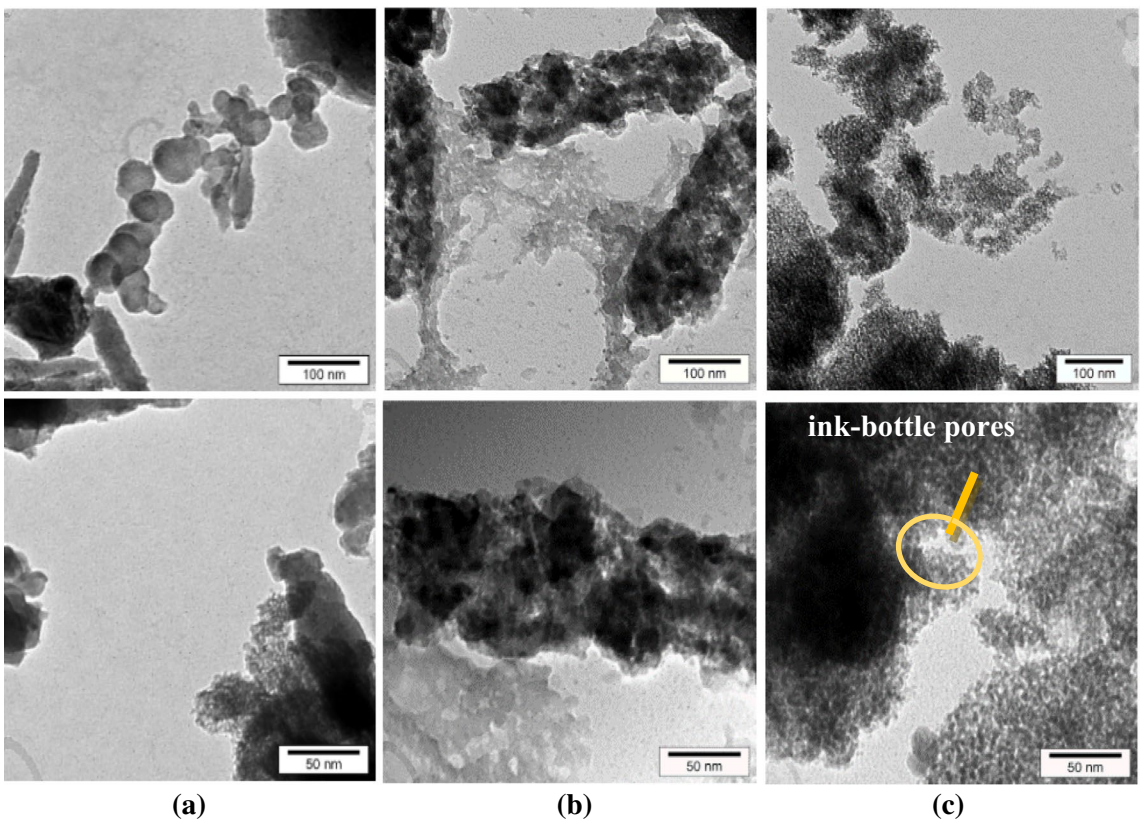

Fig. 7 TEM images of **a** $Al_{50}VC_{50}T_{350}$, **b** $Al_{50}VC_{50}T_{500}$, **c** $Al_{90}VC_{10}T_{500}$

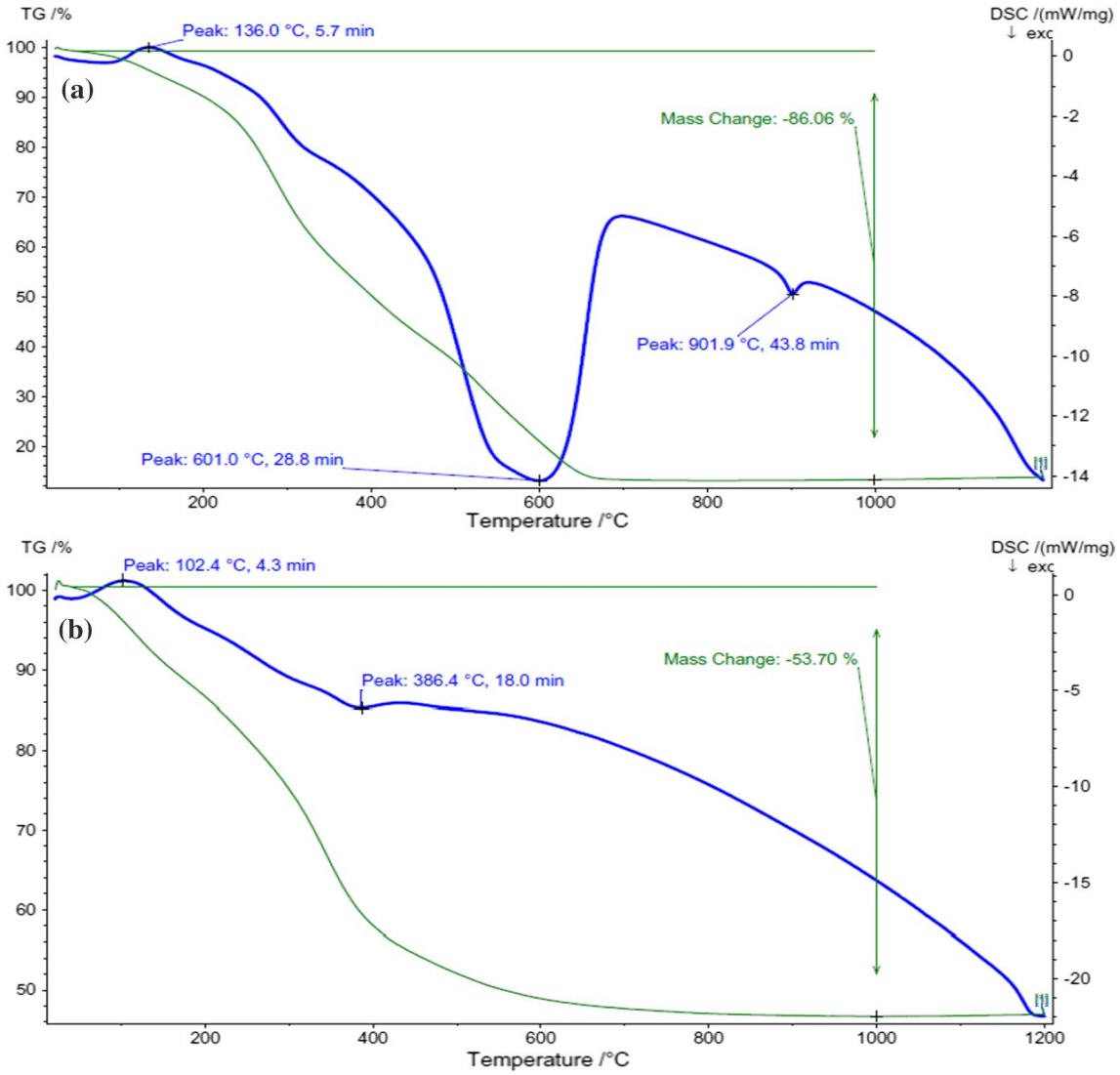

Fig. 8 TG–DSC curves of the as-prepared Al/vitamin C composites: **a** $Al_{50}VC_{50}T_{120}$, **b** $Al_{90}VC_{10}T_{120}$

loss occurred in three stages. The initial weight loss (from room temperature to 250 °C) was related to a major loss of adsorbed water (associated with the endothermic peak at 136 °C in the DSC curves) and vitamin C decomposition (Ergu et al. 2008; Ibrahim and Abu-Ayana 2009; Juhász et al. 2012; Sarkar et al. 2007). Second weight loss was observed in the range of 250–400 °C which corresponds to an exothermic peak at about 300 °C (in DSC curve) due to the dehydration of the aluminium hydroxides and continuation of vitamin C decomposition. The most noticeable weight loss, between 400 and 700 °C, corresponds to an endothermic peak in the range of 550–650 °C associated with the removal of organic residues, dehydroxylation and formation of alumina and water residue vaporization (Othman and Sahadan 2006). The broad exothermic peak between 700 and 1200 °C indicates the transformation of transition alumina to α-Al_2O_3 (Bokhimi et al. 2001; Jayaseelan et al. 1998). There was no significant weight loss for calcination temperatures above 700 °C, which implies fully elimination of all organic materials, and the stable residue can be determined as pure single-phase α-alumina.

The thermogram for $Al_{90}VC_{10}$ (Fig. 8b) shows similar three stages of weight loss. The first weight loss (from room temperature to 200 °C) was ascribed to the elimination of physically and chemically adsorbed water (associated with the endothermic peak at 102 °C in the DSC curves) and vitamin C decomposition. The second weight loss was observed in the range of 200–400 °C, and the continuation of vitamin C decomposition, which corresponds to an exothermic peak at about 386 °C (in DSC curve), was a result of the dehydration of the aluminium hydroxides. The next weight loss, between 400 and 650 °C, follows the same trend described

in the third stage of weight loss as in $Al_{50}VC_{50}$. The pattern of curves in $Al_{90}VC_{10}$ samples was similar to $Al_{50}VC_{50}$ samples in which there was no observation of paramount weight loss for temperatures higher than 800 °C and the residue was identified to be pure α-Al_2O_3. A total weight loss of 86.06 and 53.70% was observed for $Al_{50}VC_{50}$ and $Al_{90}VC_{10}$ during the thermal process, respectively. The excess weight loss for $Al_{50}VC_{50}$ is because of more vitamin C content. The maximum decomposition rate of vitamin C is 191–221 °C (Juhász et al. 2012).

In the presence of vitamin C, it was expected to see the endothermic peak around 197 °C (melting point of vitamin C). The absence of this peak in thermograms corroborates the decomposition of vitamin C before 197 °C as mentioned in FT-IR section. Clearly, these findings are consistent with the IR results, as it shows the decomposition of vitamin C below 200 °C and confirms the formation of amorphous γ-alumina by dehydroxylation due to calcination of boehmite in accordance with second weight loss observed in the range of 200–400 °C.

N_2 adsorption–desorption isotherm

Brunauer–Emmett–Teller (BET) analysis was performed to evaluate the precise specific surface area, the pore size distribution and porous nature of the Al_2O_3 samples at calcination temperatures of 250, 350 and 500 °C for 8 h. It was expected that the surface area increases by templating vitamin C. The N_2 adsorption–desorption isotherms, corresponding BJH pore size distribution curves and BET plots of mesoporous alumina are recorded in Fig. 9. Relying on the IUPAC classification of physisorption isotherms, the isotherm of all samples is classified as type IV. However, the characteristic features of these samples vary in terms of its hysteresis loop. Generally, type IV isotherms are related to complex pore interconnectivity. Many characteristics of mesoporous materials are observed in this type of isotherm where capillary condensation occurs in mesopores (Sing 1985). The N_2 adsorption hysteresis loops are indications of textural porosity (Tanev and Pinnavaia 1996). $Al_{50}VC_{50}$ samples at 250 and 350 °C (Fig. 9a, green and blue curves) exhibit a type IV isotherm with H3-type hysteresis loop. The appearance of type H3 hysteresis loops is attributed to plate-like particles slit-shaped pores. These results resemble greatly with as-prepared composites in their mesoporous appearance. The observed isotherm for $Al_{50}VC_{50}$ at 500 °C is categorized as type IV isotherm with H2-shaped hysteresis loops (Fig. 9a, red curve). In $Al_{90}VC_{10}$ samples at all temperatures, the isotherm curves (Fig. 9b) show a type IV with H2 hysteresis loops, which implies to ink-bottle pores.

The BET specific surface area, the pore volumes and the average pore diameters measurements of the Al/VC

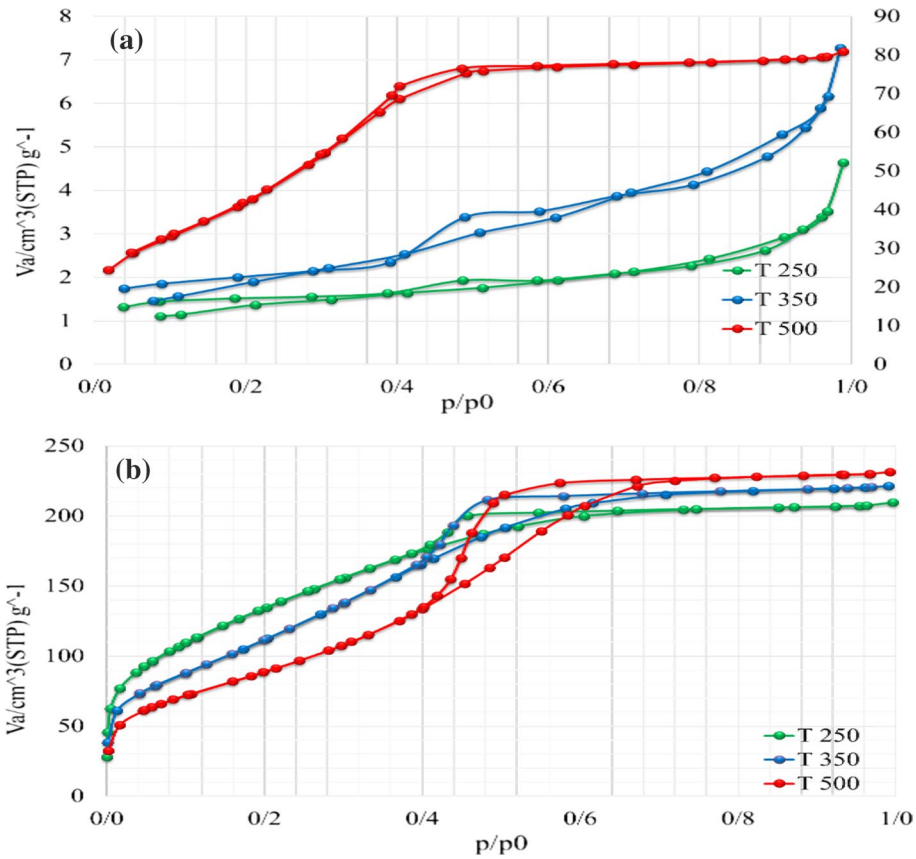

Fig. 9 N_2 adsorption–desorption isotherms of **a** $Al_{50}VC_{50}$ and **b** $Al_{90}VC_{10}$

composites in the molar ratios of 50:50 and 90:10 at calcination temperatures of 250, 350 and 500 °C are listed in Table 3. In the synthesis of Al_2O_3 process, the data show that as the proportion of vitamin C was decreased, the S_{BET} was increased, ranging from 4.9 to 480.5 m^2/g. This was related to the fact that the internal spaces of the pores are filled with vitamin C. This assumption is justified by a decrease in the pore volume. Regarding the $Al_{90}VC_{10}T_{350}$, the largest surface area for γ-Al_2O_3 is calculated to be 394 m^2/g. The average pore diameter of the Al/VC samples is in the range of 2.7–6.8 nm range. This narrow pore size distribution is of paramount value in catalytic and adsorption application.

Table 3 Textural properties of samples

Sample	S_{BET} (m^2/g)	Pore size (nm)	Pore volume (cm^3/g)
$Al_{50}VC_{50}T_{250}$	4.89	5.81	0.01
$Al_{90}VC_{10}T_{250}$	480.5	2.69	0.32
$Al_{50}VC_{50}T_{350}$	6.67	6.75	0.01
$Al_{90}VC_{10}T_{350}$	393.77	3.48	0.34
$Al_{50}VC_{50}T_{500}$	136.21	3.67	0.12
$Al_{90}VC_{10}T_{500}$	316.12	4.52	0.36

High-pressure liquid chromatography

The chirality of the columns was investigated for propranolol hydrochloride. On first successful attempt with the acetonitrile as mobile phase, the results showed the separation of enantiomers using $Al_{50}VC_{50}T_{350}$ as stationary phase. The chromatogram (Fig. 10a) showed two peaks for *R*- and *S*-isomers with R_s(resolution) about 1 (Table 4), confirming the chirality of this composite. However, the band broadening (and hence low efficiency) indicated the necessity of optimization of the process. The chromatograms of other composites showed only one peak, indicating no separation for propranolol hydrochloride enantiomers (Figs. 10b, c and d).

Optimization efforts resulted in mobile phase composed of n-hexane/ethanol/DEA (70/30/0.3, v/v/v) at a flow rate of 1.0 mL/min and 25 °C. This solution (*n*-hexane/ethanol/DEA) was mixed and filtered (≤ 0.5 µm porosity) (Fig. 11).

The chromatogram (Fig. 12) showed two peaks for *R*- and *S*-isomers with R_s (resolution) about 2.5 (Table 5), confirming the chirality of $Al_{50}VC_{50}T_{350}$ composite.

Validation of reproducibility for the columns packed with $Al_{50}VC_{50}T_{350}$ was performed via repeating the separation of propranolol hydrochloride enantiomers on $Al_{50}VC_{50}T_{350}$ as CSP under the same separation condition (Fig. 12). It is observed that the retention time, selectivity, resolution

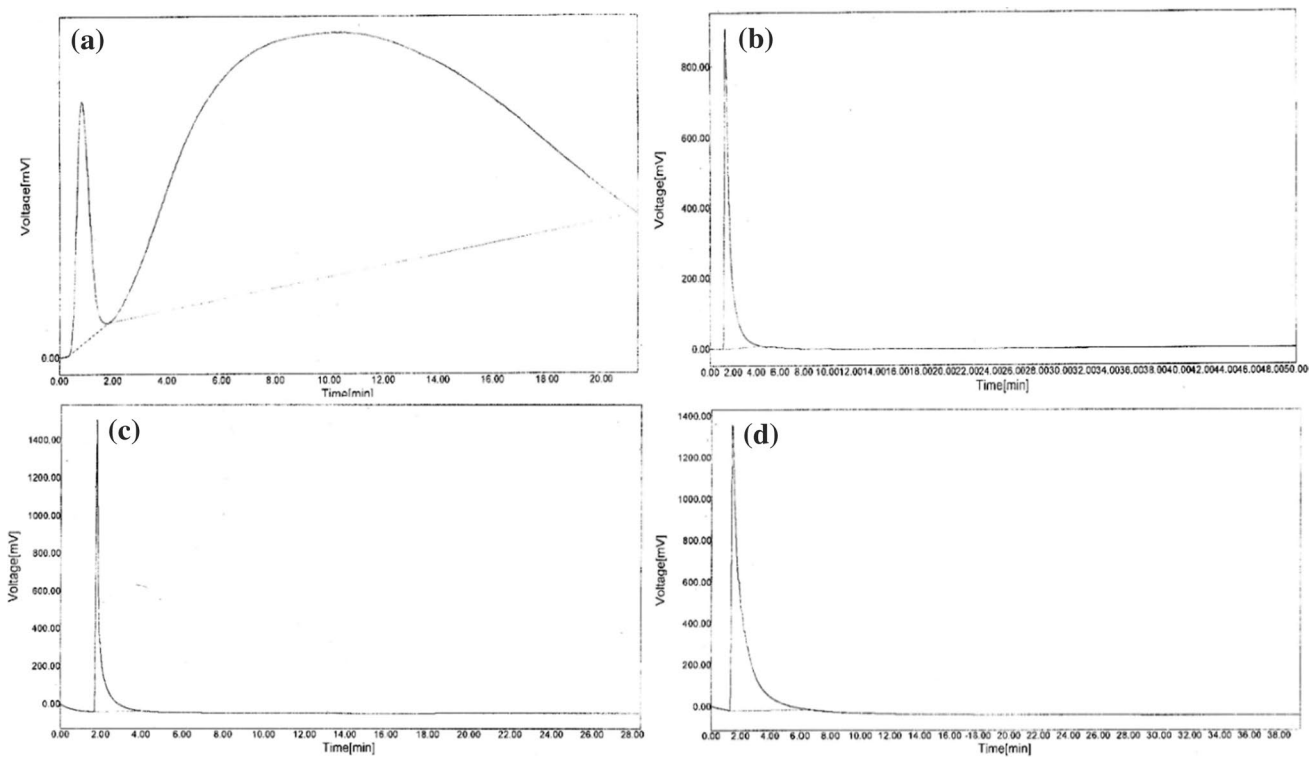

Fig. 10 Chromatograms of resolution of propranolol hydrochloride enantiomers by HPLC using **a** $Al_{50}VC_{50}T_{350}$, **b** $Al_{50}VC_{50}T_{500}$, **c** $Al_{90}VC_{10}T_{350}$, **d** $Al_{90}VC_{10}T_{500}$ as a chiral stationary phase and acetonitrile as mobile phase

Table 4 Obtained results from HPLC and the surface area of the composite (*n*-hexane/ethanol/DEA as mobile phase)

Racemate	Composite	*RT* (min)	Area (mV × s)	Height (mV)	R_S	Pore size (nm)
Propranolol hydrochloride	$Al_{50}VC_{50}T_{350}$	0.85	816.2073	25.2729	0.95	6.75
		10.2333	18975.6777	25.7603		
	$Al_{50}VC_{50}T_{500}$	1.3483	28183.7875	905.7872	–	3.67
		–	–	–		
	$Al_{90}VC_{10}T_{350}$	1.7983	20106.1797	1546.9004	–	3.48
		–	–	–		
	$Al_{10}VC_{10}T_{500}$	1.4567	63407.95	1379.1127	–	4.52
		–	–	–		

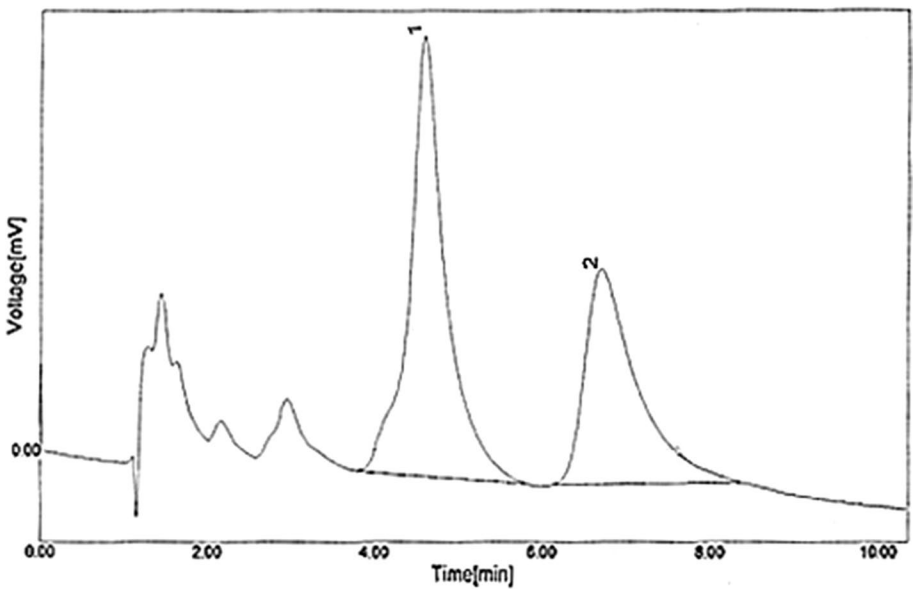

Fig. 11 Chromatograms of resolution of propranolol hydrochloride enantiomers by HPLC $Al_{50}VC_{50}T_{350}$ as a chiral stationary phase and *n*-hexane/ethanol/DEA as mobile phase

and the peak shape are kept well during the experiments, confirming the reliability of this home-made CSP (Table 6).

By considerations of the BET results, probably the pore size of the composites dominated the ability to resolving enantiomers. As $Al_{50}VC_{50}T_{350}$ has larger pore size (6.75 nm) in comparison with the other three (Table 3), it is successful in enantioseparation. Also, our calculation with GAUSSIAN G09 showed that *R*- and *S*-enantiomers of 2-propranolol have different molar volumes. The molar volume for *R*-enantiomer is 190.943 cm^3/mol, and the molar volume for *S*-enantiomer is 234.675 cm^3/mol. Therefore, one of the enantiomers fits better in the pore and the resolution occurs.

Above all, as shown in Fig. 13, propranolol hydrochloride has aromatic group that is connected to an OCH_2 group and this group (OCH_2) is connected to the chiral centre. Also, this molecule is composed of hydroxyl and amino functional groups. These functional groups have more interactions with the surface leading to chiral separation.

In conclusion, $Al_{50}VC_{50}T_{350}$ obtained in facile and green procedure is successful in resolving propranolol hydrochloride enantiomers. The potential in resolving β-blockers

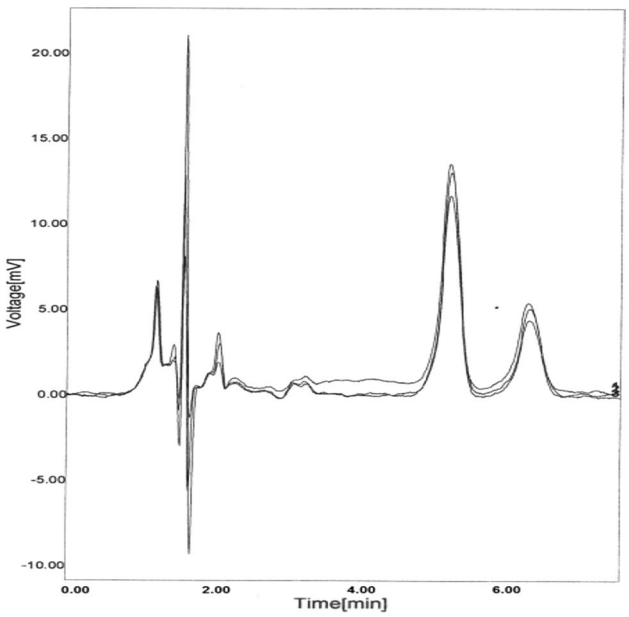

Fig. 12 Duplicate enantiomer recognition of propranolol hydrochloride enantiomers on $Al_{50}VC_{50}T_{350}$ as CSP

Table 5 Obtained results from HPLC using $Al_{50}VC_{50}T_{350}$ as CSP and the surface area of the composite (*n*-hexane/ethanol/DEA as mobile phase)

Composite	*RT* (min)	Area (mV × s)	Height (mV)	R_S	Pore size (nm)
$Al_{50}VC_{50}T_{350}$	4.5833	539.1251	17.8864	2.53	6.75
	6.70	374.4136	8.7636		

Table 6 RSD data of duplicate enantiomer recognition

Retention time RSD (%)	R_s RSD (%)
0.85	0.95

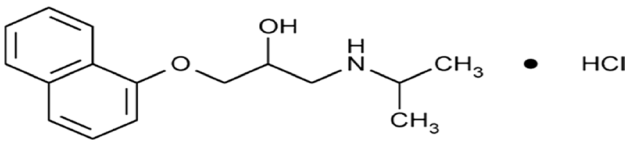

Fig. 13 Chemical structure of propranolol hydrochloride

(metoprolol, atenolol and pindolol) is expected. The study on the application of this composite in the enantiomer separation of other β-blockers is going on in our laboratory.

Conclusions

The eco-friendly and facile procedure was developed to prepare aluminas using sol–gel technique and vitamin C as a chiral template and structural directing agent. The prepared amorphous mesoporous alumina ($Al_{90}VC_{10}T_{350}$) introduce excellent capabilities, large surface area (ca. 394 m^2/g), 0.4 cm^3/g pore volume and narrow pore size distributions to be applied as catalysts. It was surprising that the $Al_{50}VC_{50}T_{500}$ composite does not resemble γ-alumina. As the quantity of vitamin C decreased from 0.5 to 0.1 molar ratios, the surface area experienced a considerable increase that resembles γ-alumina at several calcination temperatures. The potential chirality of the surface was confirmed for $Al_{50}VC_{50}T_{350}$ by using the high-performance liquid chromatography in resolving propranolol hydrochloride enantiomers. The $Al_{50}VC_{50}T_{350}$ can be used as an ideal candidate for home-made chiral stationary phase due to its green and facile preparation procedure and being inexpensive in comparison with commercial CSPs.

Acknowledgements The authors would like to thank the Isfahan University of Technology (IUT) Research Council and the Iranian Nanotechnology Initiative Council for their financial support.

References

Barrett A, Cullum VA (1968) The biological properties of the optical isomers of propranolol and their effects on cardiac arrhythmias. Br J Pharmacol 34:43–55

Barzegar-Bafrooei H, Ebadzadeh T (2011) Synthesis of nanocomposite powders of γ-alumina-carbon nanotube by sol–gel method. Adv Powder Technol 22:366–369

Bokhimi X, Toledo-Antonio J, Guzman-Castillo M, Mar-Mar B, Hernandez-Beltran F, Navarrete J (2001) Dependence of boehmite thermal evolution on its atom bond lengths and crystallite size. J Solid State Chem 161:319–326

Boumaza A et al (2009) Transition alumina phases induced by heat treatment of boehmite: an X-ray diffraction and infrared spectroscopy study. J Solid State Chem 182:1171–1176

Bowen P, Highfield JG, Mocellin A, Ring TA (1990) Degradation of aluminum nitride powder in an aqueous environmet. J Am Ceram Soc 73:724–728

Čejka J (2003) Organized mesoporous alumina: synthesis, structure and potential in catalysis. Appl Catal A General 254:327–338

Dabbagh HA, Shahraki M (2013) Mesoporous nano rod-like γ-alumina synthesis using phenol–formaldehyde resin as a template. Microporous Mesoporous Mater 175:8–15

Dabbagh HA, Zamani M (2011) Catalytic conversion of alcohols over alumina–zirconia mixed oxides: reactivity and selectivity. Appl Catal A General 404:141–148

Dabbagh HA, Taban K, Zamani M (2010) Effects of vacuum and calcination temperature on the structure, texture, reactivity, and selectivity of alumina: experimental and DFT studies. J Mol Catal A Chem 326:55–68

Dabbagh HA, Rasti E, Yalfani MS, Medina F (2011) Formation of γ-alumina nanorods in presence of alanine. Mater Res Bull 46:271–277

Ergu O, Gürü M, Cabbar C (2008) Preparation and characterization of alumina-zirconia composite material with different acid ratios by the sol-gel method Open. Chemistry 6:482–487

Gandhi MR, Viswanathan N, Meenakshi S (2010) Preparation and application of alumina/chitosan biocomposite. Int J Biol Macromol 47:146–154

Ibrahim D, Abu-Ayana Y (2009) Preparation of nano alumina via resin synthesis. Mater Chem Phys 113:579–586

Janosovits U, Ziegler G, Scharf U, Wokaun A (1997) Structural characterization of intermediate species during synthesis of Al_2O_3-aerogels. J Non-crystalline Solids 210:1–13

Jayaseelan D, Nishikawa T, Awaji H, Gnanam F (1998) Pressureless sintering of sol-gel derived alumina–zirconia composites. Mater Sci Eng A 256:265–270

Jiao WQ, Yue MB, Wang YM, He M-Y (2012) Catanionic-surfactant templated synthesis of organized mesoporous γ-alumina by double hydrolysis method. J Porous Mater 19:61–70

Juhász M, Kitahara Y, Takahashi S, Fujii T (2012) Thermal stability of vitamin C: Thermogravimetric analysis and use of total ion monitoring chromatograms. J Pharm Biomed Anal 59:190–193

Kim T, Lian J, Ma J, Duan X, Zheng W (2010) Morphology controllable synthesis of γ-alumina nanostructures via an ionic liquid-assisted hydrothermal route. Cryst Growth Des 10:2928–2933

Liu H, Ning G, Gan Z, Lin Y (2009) A simple procedure to prepare spherical α-alumina powders. Mater Res Bull 44:785–788

Morterra C, Magnacca G (1996) A case study: surface chemistry and surface structure of catalytic aluminas, as studied by vibrational spectroscopy of adsorbed species. Catal Today 27:497–532

Murali K, Thirumoorthy P (2010) Characteristics of sol–gel deposited alumina films. J Alloys Compd 500:93–95

Oberlander RK (1985) Aluminas for catalysts-their preparation and properties. Chem Inform 16:33

Othman M, Sahadan I (2006) On the characteristics and hydrogen adsorption properties of a Pd/γ-Al_2O_3 prepared by sol–gel method. Microporous Mesoporous Mater 91:145–150

Panicker CY, Varghese HT, Philip D (2006) FT-IR, FT-Raman and SERS spectra of Vitamin C. Spectrochim Acta Part A Mol Biomol Spectrosc 65:802–804

Petrovic R, Milonjic S, Jokanovic V, Kostic-Gvozdenovic L, Petrovic-Prelevic I, Janackovic D (2003) Influence of synthesis parameters on the structure of boehmite sol particles. Powder Technol 133:185–189

Potdar H, Jun K-W, Bae JW, Kim S-M, Lee Y-J (2007) Synthesis of nano-sized porous γ-alumina powder via a precipitation/digestion route. Appl Catal A 321:109–116

Priya GK, Padmaja P, Warrier K, Damodaran A, Aruldhas G (1997) Dehydroxylation and high temperature phase formation in sol-gel boehmite characterized by Fourier transform infrared spectroscopy. J Mater Sci Lett 16:1584–1587

Raman NK, Anderson MT, Brinker CJ (1996) Template-based approaches to the preparation of amorphous, nanoporous silicas. Chem Mater 8:1682–1701

Ren-Dan Z, Lai-Sheng L, Cheng B-P, Gui-Zhen N, Zhang H-F (2014) Enantioseparation and determination of propranolol in human plasma on a new derivatized β-cyclodextrin-bonded phase by HPLC. Chin J Anal Chem 42:1002–1009

Sanchez-Valente J, Bokhimi X, Toledo J (2004) Synthesis and catalytic properties of nanostructured aluminas obtained by sol–gel method. Appl Catal A General 264:175–181

Sarkar D, Adak S, Mitra N (2007) Preparation and characterization of an Al_2O_3–ZrO_2 nanocomposite, part I: powder synthesis and transformation behavior during fracture. Compos A Appl Sci Manuf 38:124–131

Sing KS (1985) Reporting physisorption data for gas/solid systems with special reference to the determination of surface area and porosity (recommendations 1984). Pure Appl Chem 57:603–619

Tanev PT, Pinnavaia TJ (1996) Mesoporous silica molecular sieves prepared by ionic and neutral surfactant templating: a comparison of physical properties. Chem Mater 8:2068–2079

Urretavizcaya G, Cavalieri A, Lopez JP, Sobrados I, Sanz J (1998) Thermal evolution of alumina prepared by the sol-gel technique. J Mater Synth Process 6:1–7

Vlaev L, Damyanov D, Mohamed M (1989) Infrared spectroscopy study of the nature and reactivity of a hydrate coverage on the surface of γ-Al_2O_3. Colloids Surf 36:427–437

Volpe L, Boudart M (1985) Topotactic preparation of powders with high specific surface area. Catal Rev Sci Eng 27:515–538

Zhang Y, Binner J (2002) Hydrolysis process of a surface treated aluminum nitride powder—a FTIR study. J Mater Sci Lett 21:803–805